On Hirth Ring Couplings: Design Principles Including the Effect of Friction

Dario Croccolo [1] , **Massimiliano De Agostinis** [1] , **Stefano Fini** [1] , **Giorgio Olmi** [1,*] , **Francesco Robusto** [1] **and Nicolò Vincenzi** [2]

[1] Department of Industrial Engineering (DIN), University of Bologna, Viale del Risorgimento 2, 40136 Bologna, Italy; dario.croccolo@unibo.it (D.C.); m.deagostinis@unibo.it (M.D.A.); stefano.fini@unibo.it (S.F.); francesco.robusto2@unibo.it (F.R.)

[2] GIULIANI, Bucci Automations S.p.A. Division, Via Granarolo 167, 48018 Faenza, Italy; n.vincenzi@bucci-industries.com

* Correspondence: giorgio.olmi@unibo.it; Tel.: +39-051-2093-455

Abstract: Rings with Hirth couplings are primarily used for the accurate positioning of axial-symmetric components in the machine tool industry and, generally, in mechanical components. It is also possible to use Hirth rings as connection tools. Specific industries with special milling and grinding machines are able to manufacture both tailor made and standard Hirth rings available on stock. Unfortunately, no international standard (for instance ISO, DIN or AGMA) is available for the production and the design of such components. In the best-case scenario, it is possible to find simplified design formulae in the catalogue of the suppliers. The aim of this work is to provide some accurate formulae and computational methods for design to provide better awareness on the limitations and the potential of this type of connection. The work consists of five parts: (i) a review of the base calculation derived mainly from the catalogues of manufacturers; (ii) an improved calculation based on a new analytical method including the friction phenomenon; (iii) an experimentation run for validating the method; (iv) a case study applied to a machine tool; and, (v) a closed form formulation to determine an upper threshold for friction, thus ensuring the Hirth coupling regular performance.

Keywords: Hirth rings; connection; serration; frontal teeth; friction; self-centering

1. Introduction

Rings with Hirth couplings (Figure 1) are based on the concept of couplings achieved by frontal teeth connections.

Figure 1. Example of Hirth rings: (**a**) disengaged and (**b**) engaged.

The concept was invented and patented by a German engineer, Carl Albert Hirth in 1928 [1]. These couplings allow obtaining very high levels of:

○　accuracy, in terms of relative positioning between the parts connected together;
○　stiffness of the system, thanks to the steady self-center geometry of the teeth;
○　power, in terms of torque transmission;
○　resistance to wear, thanks to a wide support surface of the teeth and the use of special alloyed steels.

For these reasons, Hirth connections are successfully used in many mechanical applications: machine tools, turning tables, transfer units, turbo-chargers, robotics, ship building, and, recently, also in the automotive industry. With regard to the automotive industry, it is possible to highlight the example in Figure 2, dealing with the replacement of the standard splined shaft connection by a frontal teeth connection in the wheel hub. In conventional systems, the drive torque is transferred between the wheel bearing and the axle journal by means of radial splines, which are affected by a certain amount of clearance. Loads that occur in day-to-day driving conditions produce a risk of looseness beyond the normal mounting clearance, resulting in comfort reduction and unpleasant noises and, in some cases, the failure of the bearing. On the contrary, the self-centering axial gear teeth are placed on the axle journal and fixed by the central screw. The connection remains completely clearance-free in the gear teeth during the entire service life. Proceeding this way, it is possible to achieve up to 10% weight reduction per wheel (resulting in fuel consumption reduction and higher dynamic performance of the vehicle), a simplified assembly operation, a clearance free coupling and, above all, up to 150% of the torque transmission capability.
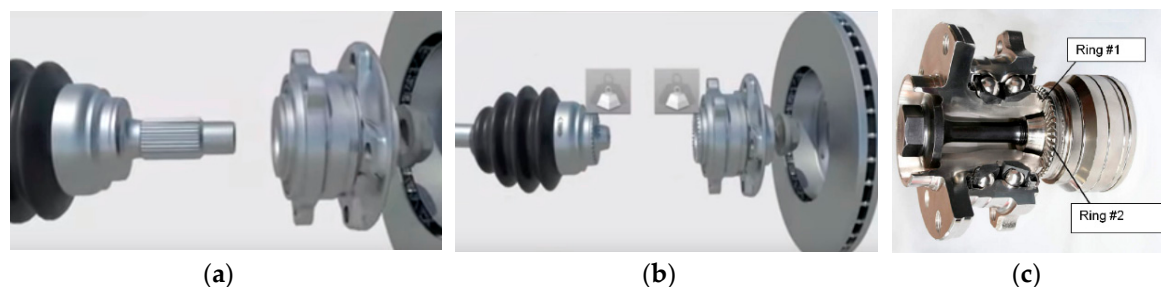

(**a**)　　　　　　　　　　　　　　　(**b**)　　　　　　　　　　　　　　　(**c**)

Figure 2. Example of Hirth connection in automotive: (**a**) old design with radial teeth and (**b**,**c**) new design with frontal teeth.

Hirth couplings, also regarded as curvic couplings, are widely used for torque transmission between mating discs in turbine machinery and are not covered by international standards (for instance ISO, DIN or AGMA). Their application makes it possible to fulfil an accurate centering, as well as an improved reliability and good structural stability. For instance, Reference [2] is focused on the structural and contact analysis of a curvic coupling in a gas turbine. In this study, a numerical model was developed to investigate the stress distribution and the contact evolution at different stages of the turbine service, in particular during preload, warm-up, speed-up, and running. The effects of coupling bolt preload, as well as of torsional load and of environmental temperature were also investigated. Other studies [3–5] have dealt with tooth contact aspects and with applications to turbo-engines in the aerospace industry [6,7].

A further interesting application of Hirth couplings, operating as servo-actuators, is in rotary tables for automatic machines and transfer machine tools [8]. These tables, fixed at predetermined angular positions, must be able to be fully constrained, thus resisting against high tangential forces. At the same time, they must have the capability of transmitting high torque, relying on tooth contact, rather than on friction couplings. Moreover, the Hirth coupling must ensure the accomplishment of strict specifications regarding the precise positioning of the rotating table, from the points of view

of its angular position and especially its centering with respect to the machine axis, after rotation. The importance of correct alignment is also highlighted in [9,10], dealing with a similar issue.

Most papers in the field of transfer machine tools or of multiple-axis automatic machines are focused on modal or dynamic analyses, such as [11,12]. This research trend is also confirmed by a recent study [13] that deals with the development and validation of a multibody dynamic model of a tool-spindle-bearing system, to be incorporated into a five-axis machine with rotary-tilting spindle heads. Conversely, the topic of the stress peak at the tooth root has not been investigated so far. Moreover, no experimental validation has ever been conducted and published in the scientific literature on numerically computed stress peaks in Hirth couplings. A further unexplored point is the relationship between the stress peak and the actual response of the Hirth connection that may be affected by several factors, such as the force acting on each tooth, the contact area, or the friction affecting the device.

The subject of the present paper is to provide an original analytical model for the Hirth coupling design with regard to the peak stress estimation and to the presence of friction. As remarked above, issues of novelty arise from the lack of similar models in the literature, focused on the actual estimation of the stress maximum value for structural assessment. A further issue of novelty arises from the inclusion of the effect of friction (between the mating teeth or on the bearing surface) in the algorithm. In fact, this is usually disregarded in the standard procedure, but its effect deserves to be considered, as it may be even detrimental for safety and accuracy. The importance of taking friction into account is also emphasized in [2], where the developed curvic coupling finite element model accounts for this item. The present study, as a further evolution, proposes an experimentally validated closed form analytical approach that can be more efficiently applied for industrial design purposes and to properly arrange scheduled maintenance.

2. Standard Calculation

Matzke [14] provided some technical data able to give a rough overview of the calculation of Hirth rings. He mainly focused his investigation on the "nominal stress" in the tooth. Based on the nomenclature of Figure 3, the total tangential force F_u (N) is applied on the mean radius R_m (mm) of the G point (center of gravity) of the tooth section and can be evaluated by Equation (1) as a function of the external torque T (Nmm) to be transmitted:

$$F_u = \frac{T}{R_m} \tag{1}$$

Neglecting the effect of friction, for a tooth angle of 60° (in Hirth connection this angle is fixed to this value) the axial force generated by the coupling is given by Equation (2):

$$F_a = F_u \cdot \tan\left(\frac{\pi}{6}\right) \tag{2}$$

The axial force can be produced, for example, by means of one or more bolts that must be accurately dimensioned [15–19]. The tooth is calculated against bending stress σ_b (MPa), approximating the trapezoidal section at the base by a rectangular one, as reported in Equation (3), where z is the number of teeth:

$$\sigma_b = \frac{6 \cdot \frac{F_u}{z} \cdot h_G}{L \cdot \left(\frac{a' + a''}{2}\right)^2} \leq \sigma_{b\_ref} \tag{3}$$

The reference values for the bending stress σ_{b_ref} (MPa) are reported in Table 1, based on the assumption of a minimum root radius (*r* > 0.3 mm [14]).
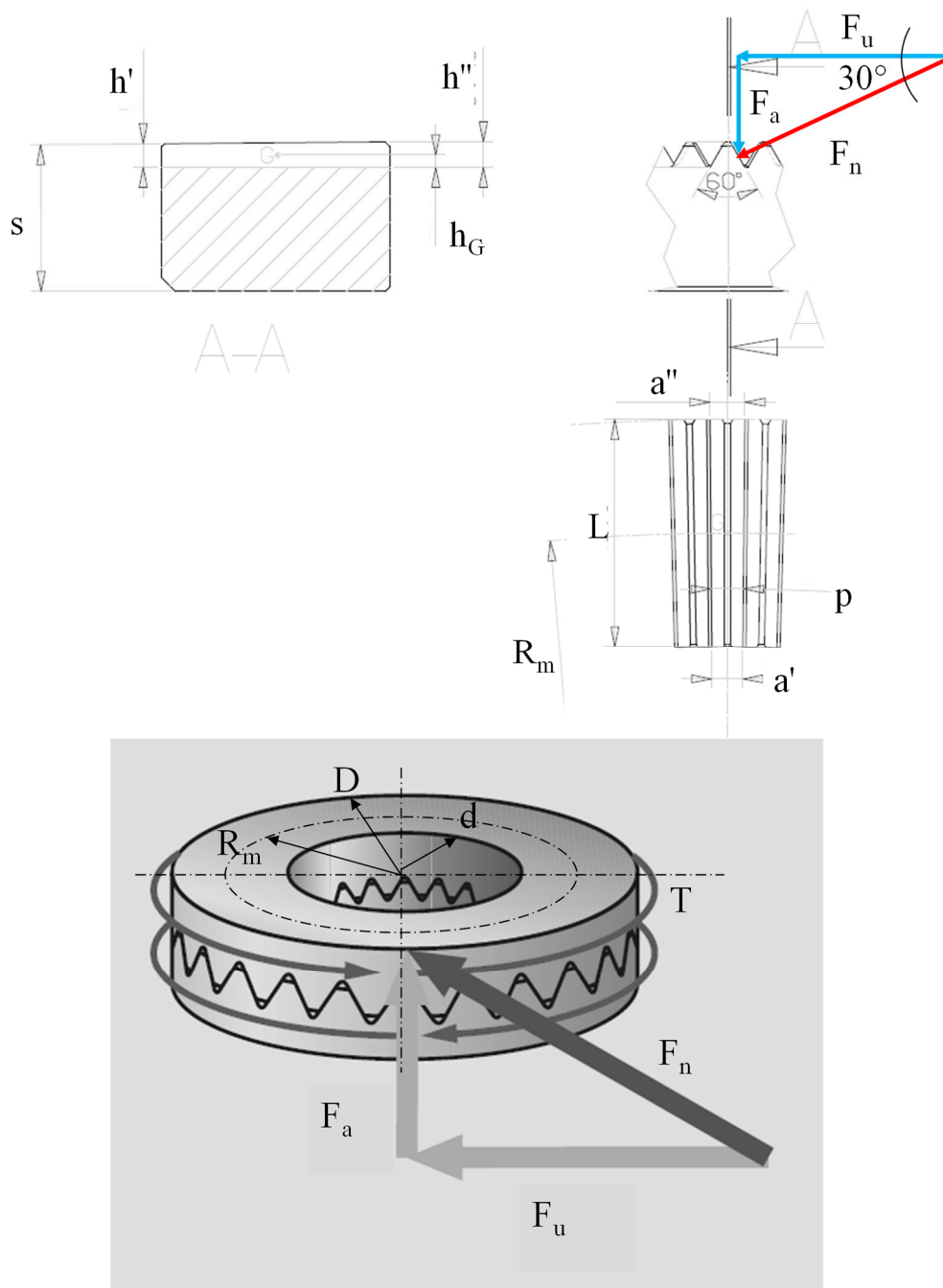
Figure 3. Nomenclature and forces acting on the tooth.

Table 1. Allowable stresses (σ_{b_ref} and $\tau_{\_ref}$) for carbon steel and for alloyed steels for base radius *r* > 0.3 mm [14,20].

Type of Stress	Carbon Steel		Alloyed Steel Cr-Ni and Cr-Mo	
	σ_{b_ref} (MPa)	$\tau_{\_ref}$ (MPa)	σ_{b_ref} (MPa)	$\tau_{\_ref}$ (MPa)
No Shocks	90	33.5	120	44.5
With shocks	50	18.5	70	26
With shocks and with torsional vibration	35	13	50	18.5

Technical German literature [20] provides a further formula in Equation (4) that is able to relate the torque T (Nmm) to the shear stress τ (MPa) to be compared to the allowable values τ_{ref} (MPa) in Table 1.

$$\tau = \frac{16 \cdot T}{\pi \cdot D^3 \left[1 - \left(\frac{d}{D} \right)^4 \right]} \leq \tau_{ref} \tag{4}$$

The maximum (peak) bending stress at the tooth base depends on the stress distribution along the tooth and on the root radius *r* (mm) at the base. The values reported in [14,20] are able to provide nominal values only, without considering the local stress concentration. These simplified formulae have, anyway, the advantage of having been fully experimentally validated. In the most recent years, the development and improvements of finite element analysis have made it possible to achieve a more accurate estimation of the actual peak stress in mechanical components under defined hypothesis [21,22]. These methods can also be suitable for frontal teeth couplings [2,5,23]. The limitation in this field is related to the lack of experimental campaigns on real components, in order to relate the stress peak to the actual response of the Hirth connection. This is likely to be affected by several factors: the force acting on each tooth, the contact area, the holes for the installation, the friction between the teeth, the heat treatment process (case hardened teeth, not always with the same hardness), the hardness gradient on the teeth and the mechanical residual stresses due to the grinding operations.

Besides the analysis of Matzke, the technical literature on Hirth rings provides some more data for the designer, which are reported below. The calculation method is based on the assumption that the external torque T (Nmm) generates the tangential force F_u (N) (Equation (1)). F_u generates, in turn, the axial force F_a (N) (Equation (2)). This axial force F_a must be absorbed by preloading devices, such as disk springs, hydraulic pistons or bolts. The required pre-load F_{v-a} (N) is calculated, introducing a safety factor ν (Equation (5)):

$$F_{v-a} = F_a \cdot \nu \quad \nu = 1.8 \ldots 3 \tag{5}$$

When compressed together, the teeth support each other if the preload F_{va} (N) is high enough. The varying loads on the tooth flanks result merely in a slightly irregular distribution of the pressure preload in the tooth root cross-section generating a maximum pressure p_{max} (MPa) according to Equation (6). In this equation (see Figure 4) A_z (mm^2) is the effective tooth flank area, D and d (mm) are the outer and the inner diameters of the teeth, d_L (mm) is the fixing hole diameter, n_b is the number of bolts in the teeth surface, *r* (mm) is the tooth root radius, s (mm) is the crown clearance, z the number of the teeth and η_z is the load bearing percentage (0.65 for milled teeth or 0.75 for grinded teeth). Under compression, with a high enough F_{va} load and with no transmission of torque, this load is equally distributed on both faces of each tooth. Conversely, when transmitting the torque T, the pressure rises on one face of the tooth and drops down on the other. The maximum pressure p_{max} (MPa) is calculated as follows:

$$\begin{cases} p_{max} = \frac{F_{v-a} + F_a}{A_z} \\ A_z = \left(D - d - \frac{n_b \cdot d_L^2}{D + d} \right) \cdot \left[\frac{\pi}{4} (D + d) - 1.155 \cdot z \cdot (r + s) \right] \cdot \eta_z \end{cases} \tag{6}$$

Concerning the geometry, the manufacturers offer a fixed parametric rule, in order to calculate the tooth height h (mm) in correspondence of the mean radius R_m (mm) (see Figure 4, Equation (7) and Table 2).
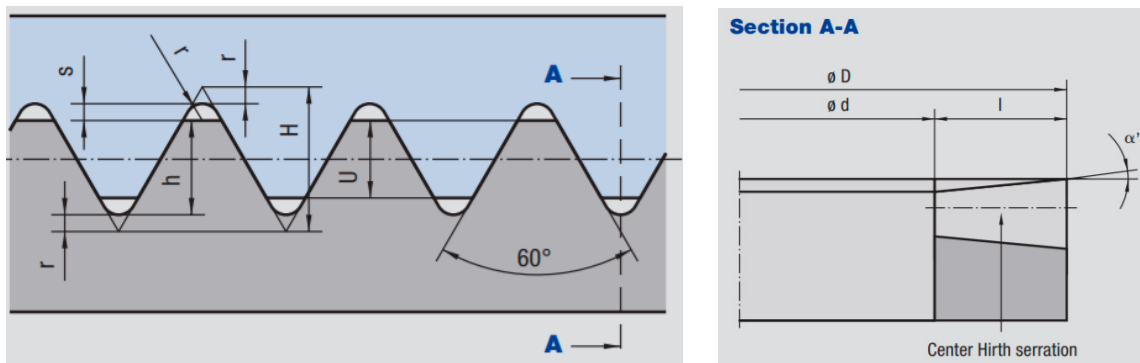
$$h = c \cdot D - (2 \cdot r + s) \tag{7}$$

Figure 4. Geometric parameters from the manufacturer "Voith-Turbo Gmbh".
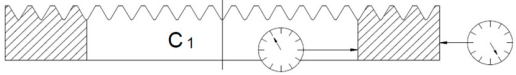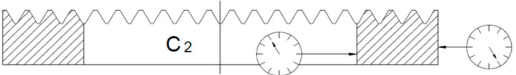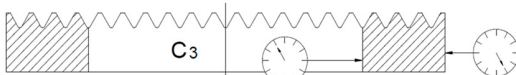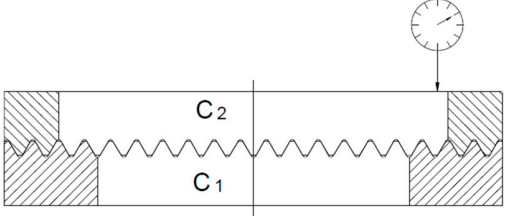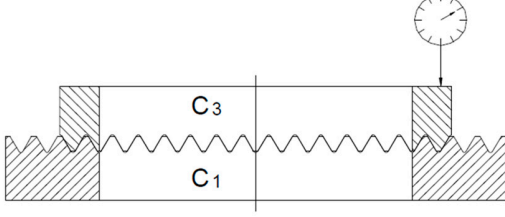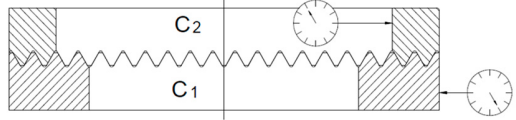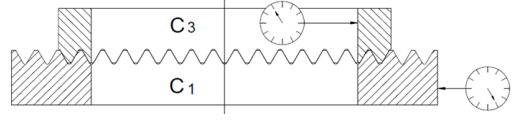
Table 2. Tables provided by the manufacturer "Voith-Turbo Gmbh" for the proper choice of Factor c and of the crown clearance s.

Number of Teeth z	Factor c
12	0.234
24	0.114
36	0.075
48	0.056
60	0.045
72	0.037
96	0.028
120	0.022
144	0.018
180	0.015
240	0.011
288	0.009
360	0.007
720	0.003

Tooth Root Radius r	Crown Clearance s
0.3	0.4
0.6	0.6
1.0	1.0
1.6	1.6
2.5	2.5

Finally, concerning Hirth ring manufacturing, the most widely used materials are alloyed steels for quenching and tempering with Cr and Mo, namely $42CrMo_4$ (W. Nr. 1.7225) or $34Cr_4$ (W. Nr. 1.7033). Their production cycle is based on the following operations: turning, drilling the fixing holes and pins, milling the teeth, inductive hardening of the tooth area (hardening in the range 52 ... 60 HRC), rough grinding of the teeth, finishing grinding of the teeth and of the reference surfaces, dimensional checking, finishing the pin holes, final checking and production of measuring report. An example of a measuring report is shown in Table 3.

The high precision and costs of these components allow an indexing accuracy of $+/-2''$ (arcsec), a repeat accuracy <0.001 mm, a self-centering capability, a high wear resistance and a long-term service life.

Table 3. Measuring report of Hirth rings engagements.

Control		Theoretical Measures	Tolerance	Results
∅ ext.	C1	990 mm	−0.01 to −0.03 mm	989.971 mm
	C2			
	C3			
∅ ext. Circularity	C1			0.005 mm
	C2			
	C3			
∅ int.	C1	849 mm H7	+0.090 mm	849.018 mm
	C2			
	C3	829 mm	+0.030 mm	829.017 mm
∅ int. Circularity	C1			0.004 mm
	C2			
	C3			0.004 mm
Concentricity ∅ int.- ∅ ext.	C1			0.003 mm
	C2			0.004 mm
	C3			0.003 mm
Flatness	C1			0.003 mm
	C2			0.002 mm
	C3			0.002 mm
Parallelism C1-C2 Rotating C2	0°			0.007 mm
	90°			0.009 mm
	180°			0.008 mm
	270°			0.009 mm
Parallelism C1-C3 Rotating C3	0°			0.008 mm
	90°			0.009 mm
	180°			0.006 mm
	270°			0.009 mm
Concentricity C1-C2 Rotating C2	0°			0.008 mm
	90°			0.009 mm
	180°			0.006 mm
	270°			0.009 mm
Concentricity C1-C3 Rotating C3	0°			0.007 mm
	90°			0.009 mm
	180°			0.008 mm
	270°			0.009 mm
Indexing accuracy				1.50''
Hardness		HRC 54	±2 (HRC)	HRC 54

3. Improved Calculation

3.1. Effect of Friction

The effect of friction between the mating teeth is not taken into account in the standard procedure. This effect is quite easy to be implemented and it is very important since it is detrimental to safety: according to Equation (8), in the presence of friction (angle of friction ρ (°)), with the same axial force, the actual transmission load $F_{u,\mu}$ (N) is reduced if the pre-load remains unchanged. Otherwise, a higher axial pre-load becomes necessary to achieve the same transmission. The coefficient of friction $\mu = \tan(\rho)$ in compression couplings can be evaluated by experimental tests, such as those reported in [24,25], and can may range between 0.1 and 0.3 for smooth surfaces.

$$\begin{cases} F_{u,\mu} = \dfrac{F_a}{\tan\left(\frac{\pi}{6}+\rho\right)} \\ F_{u,\mu} = F_u \cdot KK = \dfrac{\tan\left(\frac{\pi}{6}\right)}{\tan\left(\frac{\pi}{6}+\rho\right)} \end{cases} \tag{8}$$

In Figure 5 the reduction factor for the transmitted load (K, Equation (8)) is reported as a function of the angle of friction.
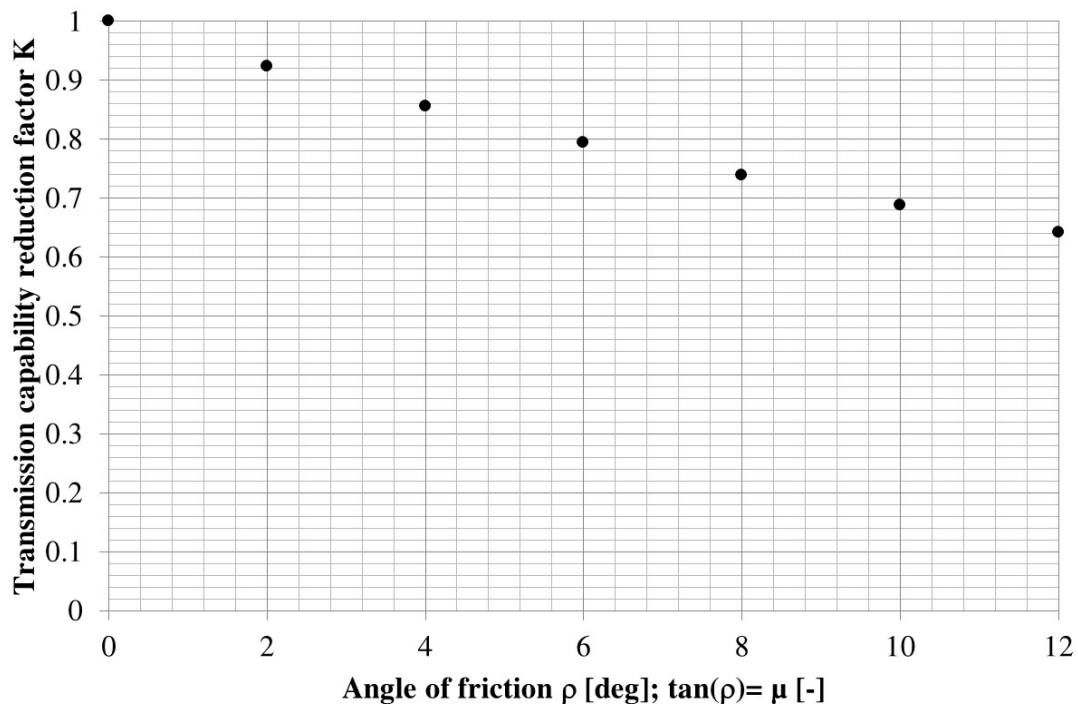
Figure 5. Reduction factor of transmission load K as a function of the angle of friction ρ.

The pressure between the teeth is also affected by the coefficient of friction, but with a lower effect. By non-linear finite element analyses (non-linear due to sliding elements in contact), it is possible to calculate the percentage reduction factor for the tooth pressure (K_p) with respect to the value calculated by Equation (6)) and, then, to plot it in the diagram of Figure 6. In the case of negligible friction ($\mu = 0$) the difference between Equation (6) and the numerical investigation is almost equal to zero.

Figure 6. Reduction factor for the tooth pressure K_p as a function of the coefficient of friction μ.

3.2. Self-Centering Capability

It is well known that Hirth connections have self-centering capability. This feature is particularly important in all the applications in which the rings must be disengaged during their life. A very common example is the turntables of the machine tools. In a multi-station round transfer machine the sequence of two actions takes place: (i) the table is fixed with the Hir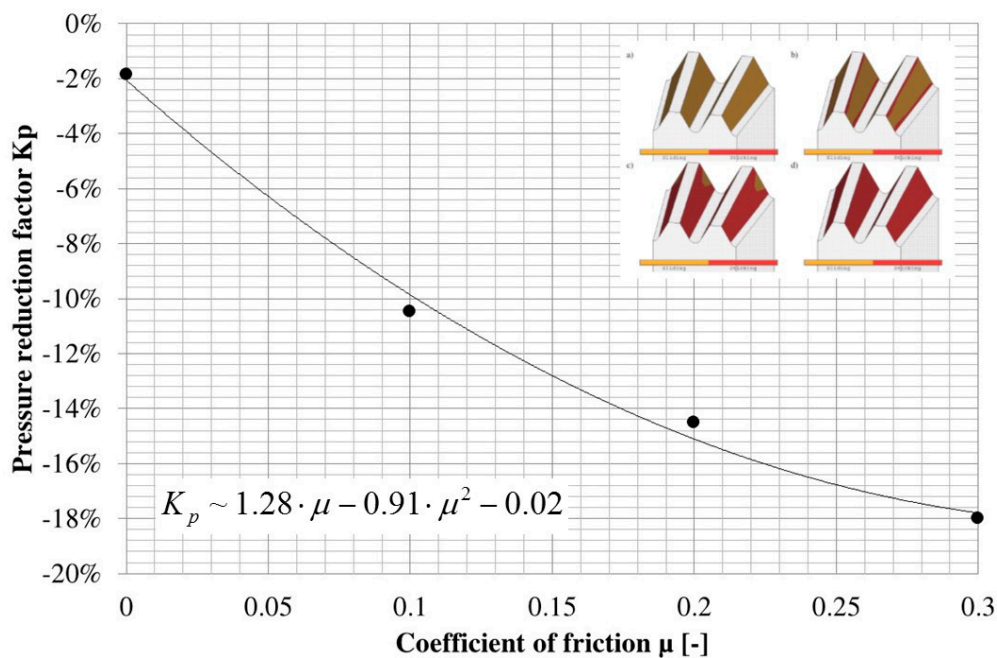th rings engaged, when the machining operations are running (the rigid connection ensures the accomplishment of the strict geometrical tolerances of the machined parts); (ii) after the end of the machining tasks in one station, the table must rotate to the next station: for this purpose, the connections must be disengaged. Following the alignment with the next station, the rotary table must then be engaged and constrained again to let new machining operations start. Repeatability, accuracy and self-centering capability are necessary to produce parts compliant with very strict geometrical tolerances. Figure 7a explains the aforementioned cycle with regard to a triple Hirth connection: ring #1 is fixed in the machine bench and it is the reference for the accurate position (it does not move). Ring #2 is connected to the rotary table, so it moves (rotates) with the table (the table must return always in the same position with respect to the machine bench). Ring #3 is responsible for engaging/disengaging and for accurate position. When ring #3 moves up, the table is disengaged and can be rotated from station to station by a motor and a gearbox. Once the table gets close to the expected position, the motor is stopped in a pre-positioning area (as the allowance in the gears of the gearbox does not allow for a precise positioning), so ring #3 can move down. During its movement from the top to the bottom, since the teeth are conical from exterior to interior (Figure 3), ring #3 initially fits the reference ring #1 (so, ring #3 is aligned with ring #1). Afterwards, it fits the movable ring #2 that is therefore taken in the correct position (so, ring#2 is also aligned with ring #1). For the correct positioning of ring #2, the axial force F_a (N) has to be high enough to move all the weight related to the rotary table on the bearing surface. The calculation of the self-centering force F_c (N), which is not provided in the technical or in the scientific literature, will be shown in the following.
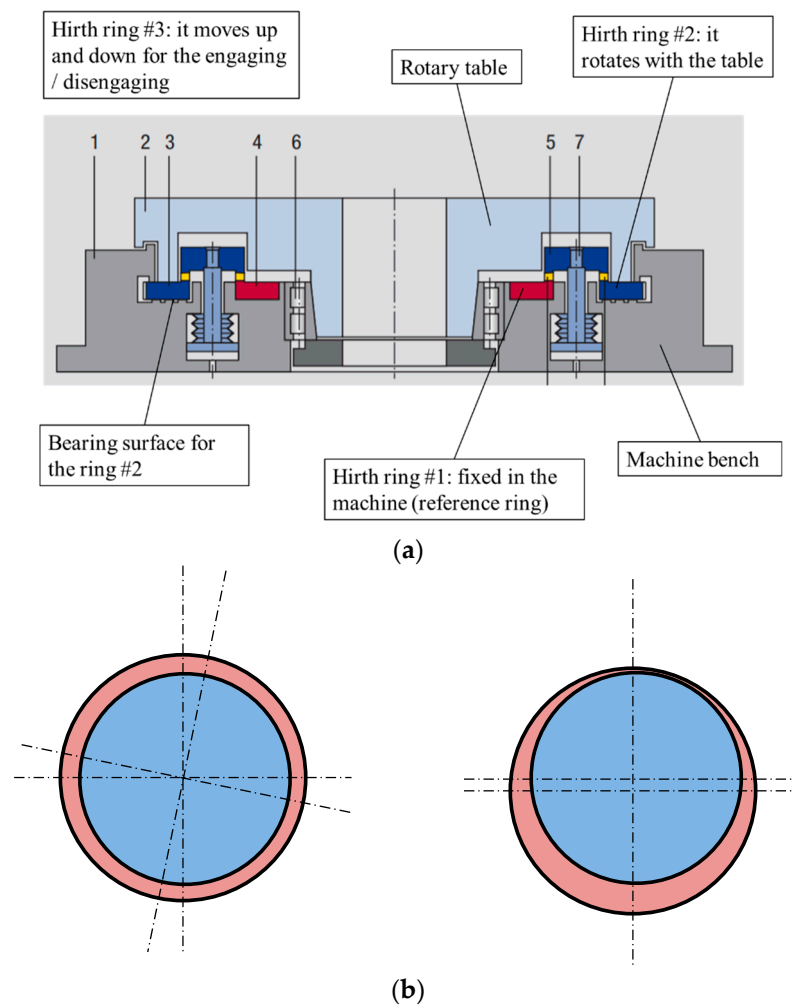
Figure 7. (**a**) Example of rotary table for the transfer machine tool; (**b**) position of ring #2 before engaging phase: left—the angle has to be adjusted; right—the center has to be adjusted.

Three possible scenarios before the engaging phase have to be considered (see Figure 7b): (i) the fixed and the rotating ring have the same center and just have a different angular position; (ii) the fixed and the rotating ring have different centers and the same angular position; (iii) a combination of (i) and (ii).

Different configurations and alignments of teeth are highlighted in Figure 8: in case (a) the teeth of the fixed and rotating rings are engaged: they are all aligned and the space between the rings is constant (the upper ring is not represented); in case (b) before the engagement of the upper ring, there is an angular misalignment of the rotating ring. Since the rings have the same center, the space between the two rings is constant. In case (c) before the engagement of the upper ring, the two centers are not aligned (the self-centering force F_c should recreate the (a) condition). As a consequence, the space between the two rings is not constant on the 360° span and furthermore an angular misalignment γ (°) of the teeth also occurs: this is variable on the 360° span.

The conditions shown in Figure 8a,b (cases a and b) do not deserve any particular analytical evaluation. Conversely, the effect of the center misalignment c (mm) (Figure 8c, case c) requires a detailed analysis. According to Figure 9, the trend of the misalignment angle γ (°) around the 360° (θ between 0° and 360°) span is yielded by Equation (9):

$$\begin{cases} r = \sqrt{R^2 + c^2 - 2 \cdot R \cdot c \cdot \cos(\theta)} \\ \gamma = \arcsin\left[\frac{c}{r} \cdot \sin(\theta)\right] \end{cases} \tag{9}$$
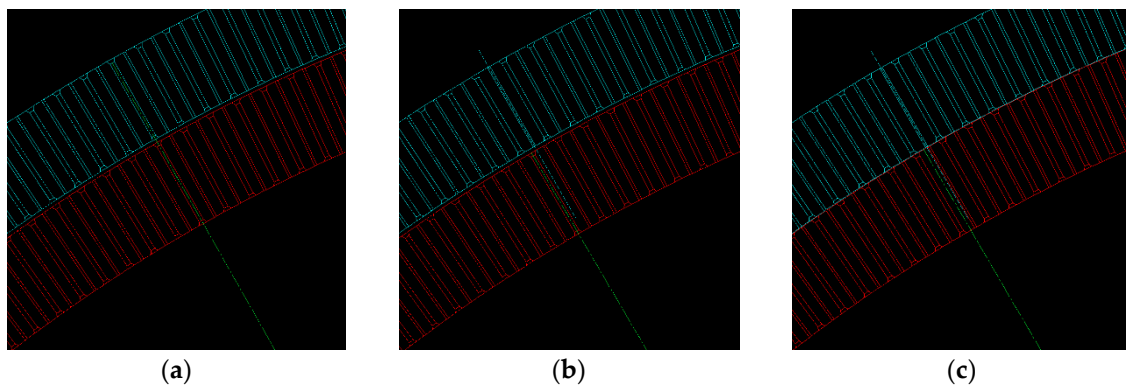
Figure 8. (**a**) Ring #1 and ring #2 engaged correctly; (**b**) before engagement: pure angular misalignment; (**c**) before engagement: center misalignment (which also generates angular misalignment).

As an example, for a ring diameter R = 450 mm, a center displacement c = 1 mm, when the angle θ is 29.5°, the angular misalignment γ is 0.063° (~4'); for θ = 89.5°, the angular misalignment γ is 0.127° (~8'). These results have also been checked by CAD system (Figure 9b). The whole trend is reported in Figure 9c for the interval 0–90°, provided that the function is symmetric every 90°.

In order to achieve the correct engagement, the following condition in Equation (10) must be fulfilled (the maximum misalignment γ must be within the angular step of the teeth):

$$\gamma_{\max} < \frac{360°}{z} \tag{10}$$

Combining Equations (9) and (10), it is possible to work out the upper threshold $c_{\max}$ (mm) for the displacement of the center of the rotating ring, in order to ensure the correct position (Equation (11)). The maximum misalignment γ for θ = 90° (see Figure 9c) is considered for processing.

$$c_{\max} = r \cdot \sin\left(\frac{360°}{z}\right) \approx R \cdot \sin\left(\frac{360°}{z}\right) \tag{11}$$

During the design phase, clearances and gaps in bearings, sealings and gears must accomplish this condition and the sum of all the assembly tolerances must be within $c_{\max}$.

Unfortunately, the condition reported in Equation (11) is not sufficient to warrant the actual occurrence of self-centering; an additional force analysis and assessment is necessary. As a matter of fact, the self-centering force F_c (N) must be high enough to overcome all the friction forces, and to consequently move the rotating ring (along with the overall mass) towards its correct position. The self-centering force F_c (N) can be calculated by means of Equation (12), where every single tooth provides a different contribution, as a function of its angular position:

$$F_c = 4 \cdot \sum_{i=0}^{z/4} \frac{F_a}{z \tan\left(\frac{\pi}{6} + \rho\right)} \cdot \sin\left(i \cdot \frac{360°}{z}\right) = K_C \cdot \frac{F_a}{\tan\left(\frac{\pi}{6} + \rho\right)} \tag{12}$$

with K_C equal to 0.642 for z = 360; 0.650 for z = 144; 0.664 for z = 72.
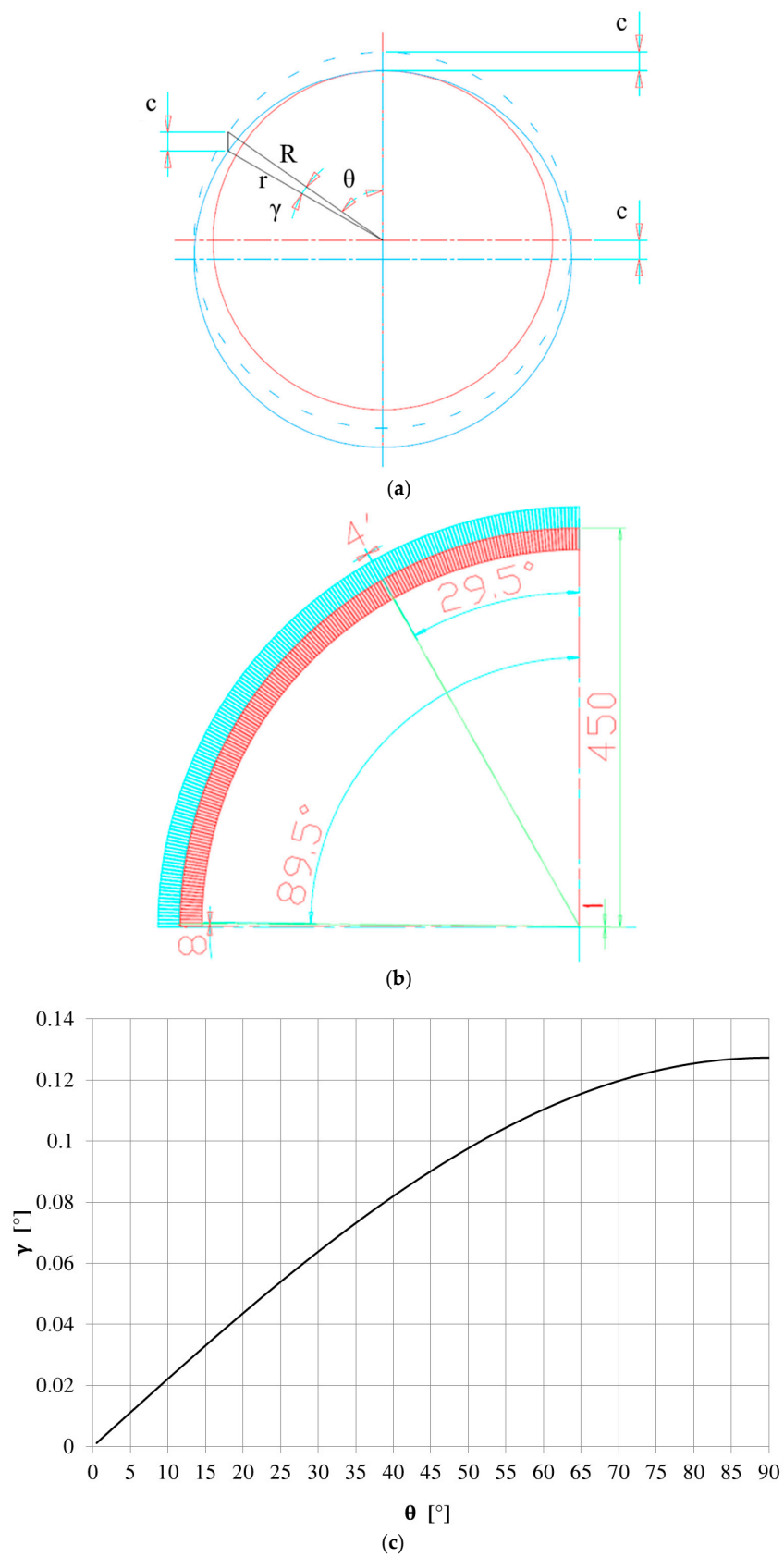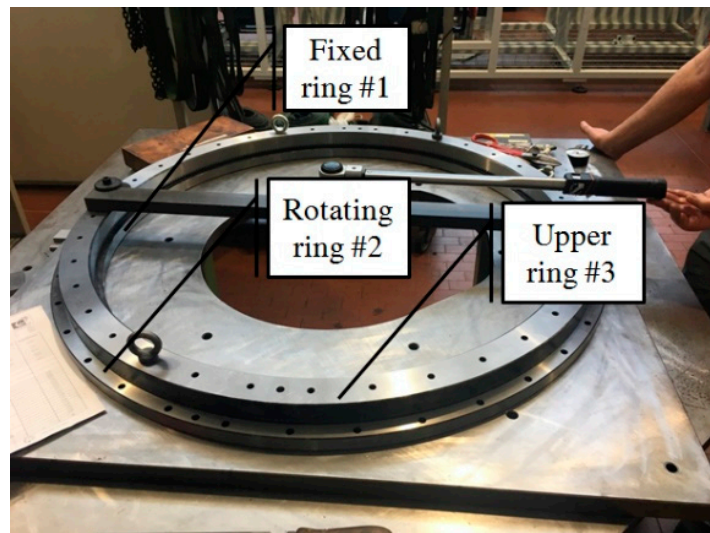
(a)

(b)

(c)

Figure 9. (**a**) Sketch for the evaluation of the misalignment angle γ; (**b**) practical example via CAD system and (**c**) related trend of γ as a function of θ.

4. Experimental Tests

Experimental tests on a triple Hirth ring connection with a mean diameter of 900 mm and z = 360 have been performed in order to check the proposed formulas (Figure 10).

	Inner Radius (mm)	Outer Radius (mm)	Weight (N)
Fixed ring #1	424.5	449	180
Rotating ring #2	450	474	250
Upper ring #3	424.5	474	310

Figure 10. Hirth ring connection with a mean diameter of 900 mm and z = 360.

At first, the static coefficient of friction μ in the bearing surface of the rotating ring (see Figure 7a) has been evaluated, in order to get its actual value. Thanks to a dynamometer, the radial force to be applied to move the rotating ring (merely supported on its bearing surface, without engagement) has been detected. The static coefficient of friction μ has therefore been calculated (five repeated tests) as the ratio between the radial force and its weight. The value of the static coefficient of friction μ is equal to 0.204 +/− 0.012; $\mu \sim 0.2$ was consequently used for the calculation. Regarding the own weight of the upper ring (310 N) as the axial pre-loading force, F_a, and considering the angle of friction ρ between the teeth of 11.3° ($\mu = 0.2$), a self-centering force $F_c = \sim225$ N is yielded by Equation (12). The frictional resistance force R_μ (N) can be evaluated as the overall sum of the weights of the rotating and upper rings (i.e., the rings that must be moved into the correct position, leveraging the position of the fixed ring), multiplied by the aforementioned coefficient of friction in the bearing surface; a force $R_\mu = \sim112$ N is determined (reference sketch in Figure 11). The experimental test has shown the self-centering capability: the rings were able to shift to the correct engaged position, being $F_c > R_\mu$. To fully validate the correctness of the formulation, an additional external force in the radial direction $F_{r,e}$ (N) has been applied and measured by the same dynamometer (Figure 12). This force can be directly combined with the frictional force R_μ (it can be regarded as an extra-frictional force), because it is able to work against the self-centering force Fc. In this way, the self-centering capability has been evaluated accurately, step-by-step increasing the force $F_{r,e}$, until ($R_\mu + F_{r,e}$) equalized the available F_c. The retrieved results are reported in Table 4; it can be highlighted that up to $F_{r,e} = 100$ N, the self-centering force is able to move the rings into the correct position, whereas in the range between $F_{r,e}$ = 100 and 120 N, the self-centering capability is equal to the resistance forces: therefore, no movement occurs. As a matter of a fact, the calculated value of Fc = ~225 N (Equation (12)) is reliable since the addition of R_μ and $F_{r,e}$ yields $\sim 112 + 120 = 232$ N.
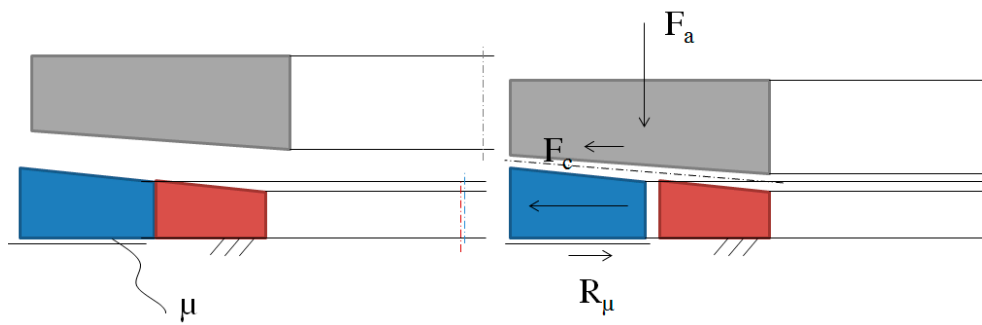
Figure 11. Hirth self-centering action.

Figure 12. Self-centering capability with the presence of R_μ and $F_{r,e}$.

Table 4. Experimental verification of the self-centering capability.

Additional External Radial Load $F_{r,e}$ (N)	Self-Centering Capability (YES/NO)
20	YES 🙂
40	YES 🙂
60	YES 🙂
80	YES 🙂
100	YES 😐
120	NO 🙁

5. Case Study

The case study proposed in this section refers to the rotary table of a big transfer machine tool, which has a Hirth ring connection with the same geometrical dimensions of that tested in the previous section. The present work moves from some issues related to the actual positioning of the rotary table (with concern regarding the loss of self-centering capability) after several years of work. After disassembling the rotary table, it was found that a lot of rust was present both in the teeth and in the bearing surface of the rotating ring (Figure 13). The presence of rust, as highlighted in [24,25], significantly increases the coefficient of friction, therefore reducing performance and self-centering capability. In this section, the aforementioned analytical predictive model is applied and the influence of the coefficient of friction on the actual performance is also studied.
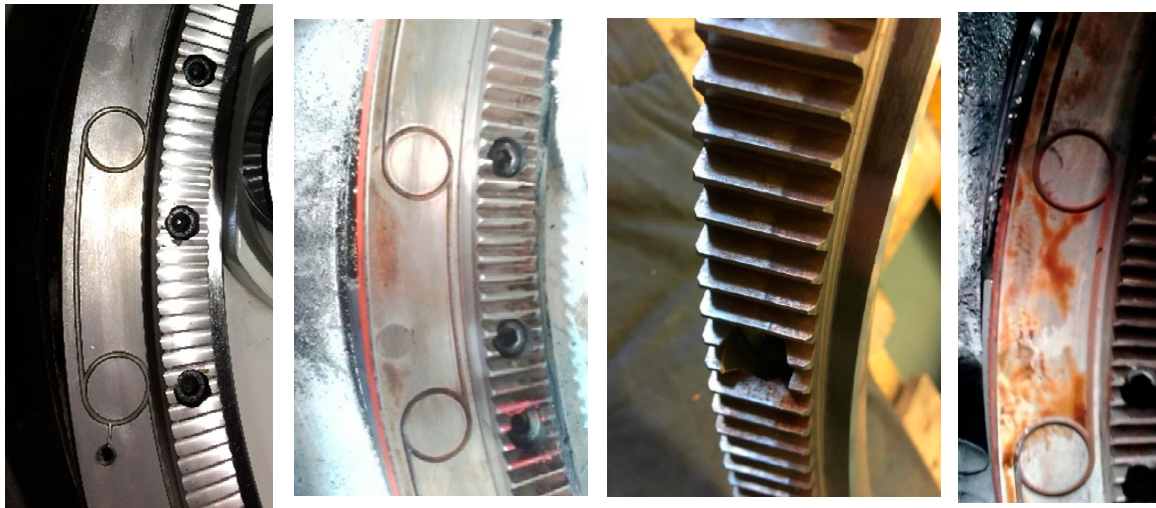
Figure 13. Comparison between the status of a new Hirth connection vs. a rusty one.

The data for the calculation are reported in Table 5.

Table 5. Calculation data for a rotary table of a transfer machine (Figure 7a).

ID	Description	Type of Data	Value	Units
1	Tooth Angle	Input data (fixed for Hirth connection)	30	°
2			0.524	rad
3	Friction angle	Input data	11.5	°
4			0.201	rad
5	Coefficient of friction μ	Calculated: $\mu = \tan(\rho)$	0.203	
6	Maximum external tangential force to be transmitted during a milling operation	Input data	5000	N
7	Distance from the center of the tangential force (radius of the rotary table)	Input data	700	mm
8	Minimum Torque T to be transmitted	Calculated: ID6 $\times$ ID7	3500	Nm
9	Hirth rings mean radius	Input data	450	mm
10	Tangential force F_u on the Hirth connection	Calculated: ID8 $\times$ 1000/ID9	7778	N
11	Safety factor SF	Input data (reference value: 3 ... 5)	4	
12	Tangential force F_u on the Hirth connection including SF	Calculated: ID10 $\times$ ID11	31,111	N
13	Tangential force F_u used for the design	Selected by the designer on the basis of ID12	35,000	N
14	Axial force F_a (including friction)	Calculated (info in the paper)	30,965	N
15	Self-centering capability F_c	Calculated (info in the paper)	22,326	N
16	Weight of the rotary table connected to the rotary ring	Input data	40,000	N
17	Frictional force R_μ	Calculated: ID16 $\times$ ID5	8138	N
18	Mean sliding radius of the bearing surface	Input data	470	mm
19	Frictional torque on the bearing surface	Calculated: ID17 $\times$ ID18	3825	Nm
20	Additional frictional torque (sealings, bearings, ...)	Input data	3000	Nm
21	Torque T that Hirth rings can transmit	Calculated: ID13 $\times$ ID9	15,750	Nm
22	Frictional torque T_μ	Calculated: ID19 + ID20	6825	Nm

Analyzing the data in Table 5, based on force balance, it is possible to highlight that the following conditions are fulfilled in the presence of a coefficient of friction μ = ~0.2 (ID5).

- The condition of the minimum torque T to be transmitted (ID8) is satisfied with the requested safety factor (SF = 4, ID11): 15,750 Nm > 3500 Nm (ID21 > ID8). The same condition also applies (obviously) to the tangential forces F_u: 35,000 N > 7778 N (ID13 > ID10).
- The axial force F_a required for the transmission of the torque is 30,965 N (ID14): it is granted by a hydraulic piston (upon setting the pressure level of the oil, this force is fixed).
- The frictional force R_μ, depending on the weight of the rotary table (40,000 N, ID16) and on the coefficient of friction (~ 0.2, ID5), is 8138 N. The self-centering capability is verified since the condition $F_c > R_\mu$ is satisfied (22,326 N > 8138 N, ID15 > ID17).
- The accuracy of the angular positioning is also verified. The friction torque on the bearing surface of the rotating ring, which depends on the frictional force R_μ, on the mean sliding radius (ID18) and on the coefficient of friction (ID5), is 3825 Nm; the additional frictional torque for the rotating elements (such as rotary sealings for oil distribution, bearings and gears) is 3000 Nm (ID20). The torque T that the Hirth connection is able to provide proves to be higher than the total frictional torque T_μ: 15,750 Nm > 6825 Nm (ID21 > ID22).

Concerning the stress analysis, it is easy to run this by Equation (3) or (4), with the teeth geometry reported in Figure 14 and considering the full torque capability T = 15,750 Nm. The equations above yield: σ_b = 0.23 MPa and τ = 0.60 MPa, which are very far from their admissible thresholds (50 MPa and 18.5 MPa respectively, Table 1).
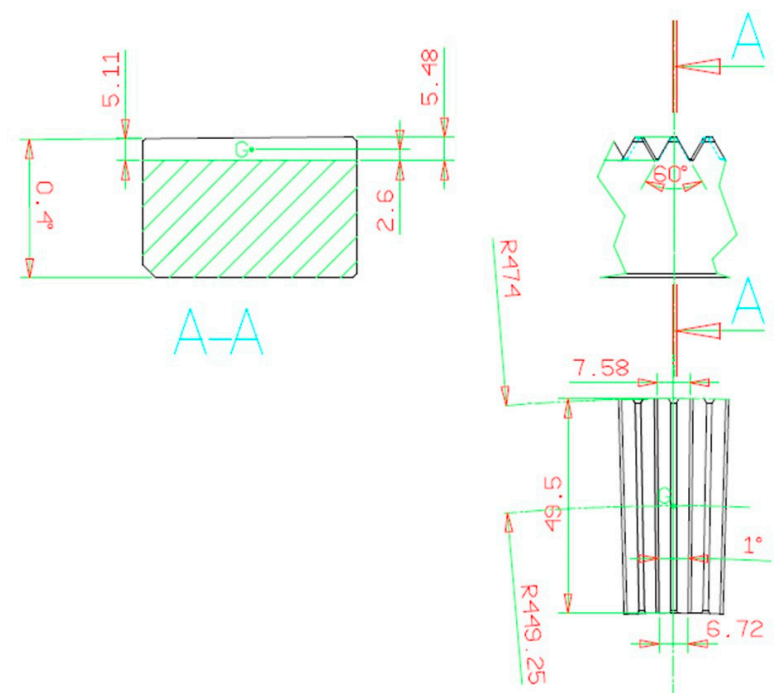
Figure 14. Tooth geometry for the case study.

Finally, the effect of the coefficient of friction is shown. According to [24,25], the coefficient of friction is strongly affected by the presence of the rust, which makes it increase. For this reason, a sensitivity analysis has been performed. The axial force F_a has not been modified, provided that the system works with a hydraulic piston set at a fixed pressure level and is able to provide F_a = 30,965 N (ID14). $F_{u,\mu}$ is therefore recalculated by Equation (8), depending on the actual value of the friction angle ρ. The other forces depending on friction are also re-calculated. The results are reported in the chart of Figure 15 and in Table 6, where the double effect of the increase of the coefficient of

friction is well visible; on one hand, it reduces the capability of the active (self-centering) forces and on the other, it increases the resistance (frictional) forces. In the proposed case study, the detrimental effect of rust is very clear: an increase of the coefficient of friction from its initial value of ~ 0.2 (for new surfaces in contact) to a value of 0.4 (or more for the rusted ones) results in the complete loss of the positioning capability of the Hirth connection for the rotary table. This in turn implies the loss of accuracy and precision in the production of the components manufactured by the transfer machine tool. When this situation occurs, the machine tool requires maintenance.
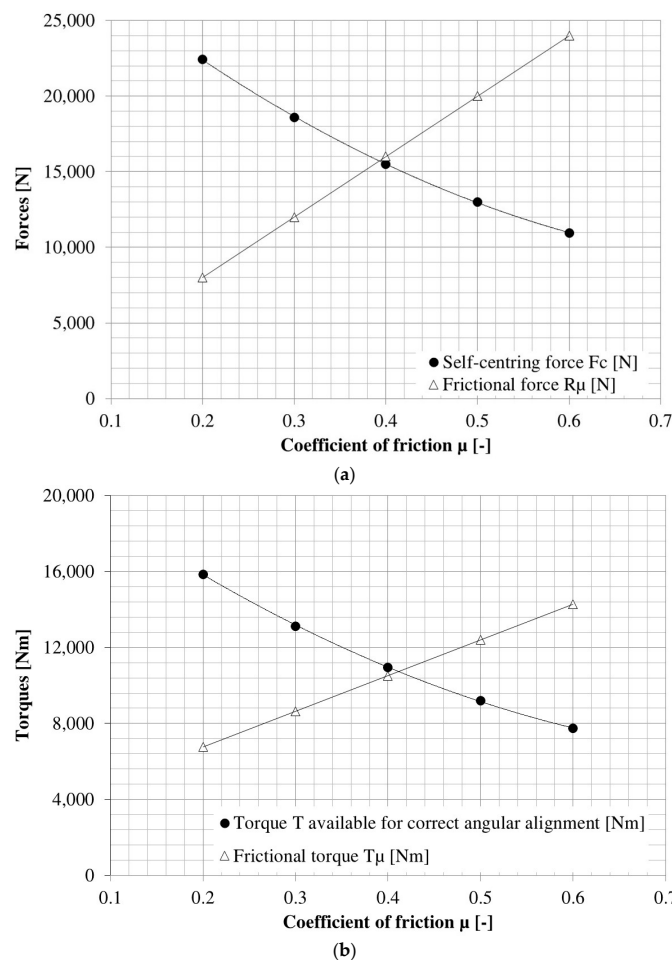

(a)

(b)

Figure 15. Sensitivity analysis with the coefficient of friction for (**a**) forces and (**b**) torque.

Table 6. Sensitivity analysis for different values of the friction coefficient.

| Coefficient of Friciton μ | Angle of Friction ρ (°) | Axial Force F_a from Hydraulic Piston (N) | Active Actions Provided by the Hirth | | | Resistance Actions Due to Friction | | Check | |
			Tangential Force F_u (N)	Self-Centering Force F_c (N)	Torque Available for Correct Angular Alignment (Nm)	Frictional Force R_μ (N)	Frictional Torque T_μ (Nm)	$F_c > R_\mu$	$T > T_\mu$
0.200	11.3		35,234	22,431	15,855	8000	6760	YES	YES
0.300	16.7		29,181	18,577	13,131	12,000	8640	YES	YES
0.400	21.8	30,965	24,366	15,512	10,965	16,000	10,520	NO	YES
0.500	26.6		20,445	13,016	9200	20,000	12,400	NO	NO
0.600	31.0		17,190	10,944	7735	24,000	14,280	NO	NO

6. Closed-Form Determination of a Friction Threshold to Ensure Self-Centering

The outcome of the previous analysis suggests the existence of an upper threshold for friction. For a fixed Hirth geometry, this depends on the applied axial force, F_a, and on the actual overall weight to be moved, W. When friction at the interface is lower than this threshold, the centering force is able

to warrant full alignment. Conversely, when friction is above this level, due to wear or rust, the axial force is no longer sufficient to allow centering.

Considering Equation (12), the friction threshold can be determined by imposing that the centering force, F_c, is greater than the frictional force arising from the weight to be moved, R_μ. This condition is highlighted in Equation (13), where μ indicates the frictional coefficient and ρ the corresponding frictional angle:

$$F_c = K_c \cdot \frac{F_a}{\tan\left(\frac{\pi}{6} + \rho\right)} \geq R_\mu = \mu \cdot W = tg(\rho) \cdot W \tag{13}$$

Some simple algebraic operations yield the solution in terms of the upper threshold for the frictional coefficient, μ_{th}:

$$\mu_{th.} = \frac{-\frac{\sqrt{3}}{3}(K_cF_a + W) + \sqrt{\frac{1}{3}(K_cF_a + W)^2 + 4WK_cF_a}}{2W} \tag{14}$$

This threshold is plotted in Figure 16, as a function of the applied axial force, for different overall weights to be moved for $K_C = 0.642$ ($z = 360$). It can be observed that $\mu_{th.}$ exhibits a non-linear increasing trend. The higher the axial force that can be transmitted by the third ring, the higher the frictional threshold, which even tends to unity. Remarkably high values of $\mu_{th.}$ clearly indicate that the frictional force component can be always easily overcome by the centering force, regardless of the presence of rust or wear. In addition, the higher the weight to be moved, the lower the retrieved threshold. This outcome indicates that, when large masses have to be centered, remarkably high axial forces are required to overcome friction, even for a low frictional coefficient at the interface. Finally, it is interesting to observe that the results in the diagram below are consistent with those of the case study above. In fact, for an axial force of around 31 kN and a weight of 40 kN, the friction threshold is 0.395. This result confirms the unverified condition for centering, as μ increases up to 0.4, as shown in Table 6.
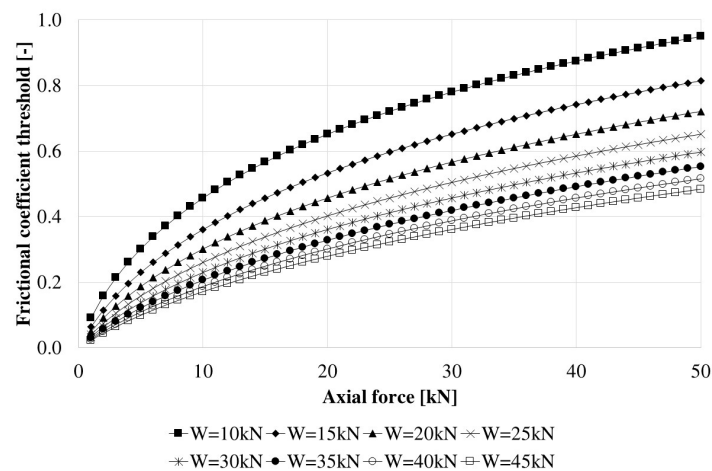

Figure 16. Friction threshold and its dependence on the axial force and the weight to be moved.

7. Conclusions

This paper presents a methodology for the precise calculation of the forces generated in Hirth ring connections. The role of friction is taken into account and is demonstrated to be fundamental for the correct calculation of this type of component. Simplified formulae in scientific or technical literature are not sufficiently accurate to describe the performance of Hirth rings in full detail. Starting from a practical example that occurred in a working machine tool that lost the accuracy of its positioning capability, some more advanced design formulae have been proposed. These novel equations have also been experimentally verified. Friction conditions are likely to change during the lifespan of a machine tool, mainly due to wear, rust and corrosion. Therefore, the designer needs to use a reliable design

method for Hirth connection calculations for long-term life. The developed model, which incorporates the effect of friction, is very important to predict the capability of the connection, and also indicates the related friction thresholds to achieve self-centering and adequate torque transfer.

Author Contributions: Conceptualization, D.C. and N.V.; Data curation, M.D.A., S.F., F.R. and N.V.; Formal analysis, G.O. and N.V.; Investigation, M.D.A., S.F. and N.V.; Methodology, D.C., M.D.A., S.F., G.O. and N.V.; Project administration, D.C. and N.V.; Supervision, D.C., G.O. and N.V.; Validation, N.V.; Writing—original draft, G.O. and N.V.; Writing—revised version, G.O., F.R. and N.V.

Nomenclature

A_z	Effective tooth flank area (mm^2)
a', a'', h_G	Geometrical features of the Hirth ring and related teeth (from Figure 3)
c	Center misalignment between the fixed and the rotating rings (mm)
c_{max}	Maximum center misalignment between the fixed and the rotating rings (mm)
D	Outer diameter of the teeth (mm)
d	Inner diameter of the teeth (mm)
d_L	Fixing hole diameter (mm)
Factor c	Factor depending on the number of teeth z (from Table 2)
F_a	Axial force generated by the Hirth coupling (N, kN)
F_c	Self-centering force (N, kN)
$F_{r,e}$	Additional external force in the radial direction (experimental validation test) (N)
FS	Safety factor for the total tangential force (-)
F_u	Total tangential force (N, kN)
$F_{u,\mu}$	Actual tangential force (including friction) (N, kN)
$F_{\nu\text{-}a}$	Preload (N, kN), considering a safety factor ν
h	Tooth height (mm)
K	Reduction factor for the transmitted load (-)
K_C	Coefficient for the self-centering force computation, depending on the number of teeth
K_p	Percentage reduction factor for the tooth pressure (%)
n_b	Number of bolts in the teeth surface
p_{max}	Maximum pressure on tooth flank (MPa)
R	Ring diameter (mm)
R_m	Mean radius of the ring (mm)
R_μ	Frictional resistance force (N, kN)
r	Tooth base radius (mm)
s	Crown clearance (mm)
T	External torque to be transmitted (Nm, Nmm)
T_μ	Frictional torque (Nm, Nmm)
W	Overall weight to be moved upon self-centering (N, kN)
z	Number of teeth (-)
γ	Angular misalignment between the fixed and the rotating rings (°)
γ_{max}	Maximum angular misalignment between the fixed and the rotating rings (°)
η_z	Load bearing percentage (-)
μ	Coefficient of friction (-)
μ_{th}	Coefficient of friction upper threshold to achieve self-centering (-)
ν	Safety factor for preload (-)
θ	General angular coordinate over the Hirth ring (°)
ρ	Angle of friction (°, rad)
σ_b	Tooth bending normal stress (MPa)
σ_{b_ref}	Allowable normal stress (MPa)
τ	Shear stress due to the transmitted torque (MPa)
$\tau_{\_ref}$	Allowable shear stress (MPa)

References

1. Hirth, C.A. Shaft Coupling. U.S. Patent 1,660,792, 28 February 1928.
2. Yuan, S.X.; Zhang, Y.Y.; Zhang, Y.C.; Jiang, X.J. Stress distribution and contact status analysis of a bolted rotor with curvic couplings. *Proc. I. Mech. Eng. C-J. Mec.* **2010**, *224*, 1815–1829. [CrossRef]
3. Pisani, S.R.; Rencis, J.J. Investigating CURVIC coupling behavior by utilizing two- and three-dimensional boundary and finite element methods. *Eng. Anal. Bound. Elem.* **2000**, *24*, 271–275. [CrossRef]
4. Richardson, I.J.; Hyde, T.H.; Becker, A.A.; Taylor, J.W. A validation of the three-dimensional finite element contact method for use with curvic couplings. *Proc. Inst. Mech. Eng. G-J. Aerosp. Eng.* **2002**, *216*, 63–275. [CrossRef]
5. Richardson, I.J.; Hyde, T.M.; Becker, A.A.; Taylor, J.W. A three-dimensional finite element investigation of the bolt stresses in an aero-engine curvic coupling under a blade release condition. *Proc. Inst. Mech. Eng. G-J. Aerosp. Eng.* **2000**, *214*, 231–245. [CrossRef]
6. Yin, Z.Y.; Hu, B.A.; Wu, J.G.; Xu, Y.L.; Zheng, Q.X. Calculation of axial relaxed/pressed forces of rotors with curvic couplings. *Acta Aeronaut. Aeronaut. Sin.* **1996**, *17*, 555–560.
7. Hu, B.A.; Yin, Z.Y.; Xu, Y.L. Determination of axial preloads of rotor with curvic couplings pretightened into two segments. *J. Mech. Strength* **1999**, *21*, 274–277.
8. Croccolo, D.; Cavalli, O.; De Agostinis, M.; Fini, S.; Olmi, G.; Robusto, F.; Vincenzi, N. A Methodology for the Lightweight Design of Modern Transfer Machine Tools. *Machines* **2018**, *6*, 2. [CrossRef]
9. Cao, H.; Li, D.; Yue, Y. Root Cause Identification of Machining Error Based on Statistical Process Control and Fault Diagnosis of Machine Tools. *Machines* **2017**, *5*, 20.
10. Zhang, F.P.; Lu, J.P.; Tang, S.Y.; Sun, H.F.; Jiao, L. Locating error considering dimensional errors modeling for multistation manufacturing system. *Chin. J. Mech. Eng.* **2010**, *23*, 765–773. [CrossRef]
11. Du, C.; Zhang, J.; Lu, D.; Zhang, H.; Zhao, W. A parametric modeling method for the pose-dependent dynamics of bi-rotary milling head. *Proc. Inst. Mech. Eng. B-J. Eng. Manuf.* **2018**, *232*, 797–815. [CrossRef]
12. Liu, X.; Yuan, Q.; Liu, Y.; Gao, J. Analysis of the stiffness of hirth couplings in rod-fastened rotors based on experimental modal parameter identification. In Proceedings of the ASME Turbine Technical Conference and Exposition, Düsseldorf, Germany, 16–20 June 2014.
13. Du, C.; Zhang, J.; Lu, D.; Zhang, H.; Zhao, W. Coupled Model of Rotary-Tilting Spindle Head for Pose-Dependent Prediction of Dynamics. *J. Manuf. Sci. Eng.* **2018**, *140*, 081008. [CrossRef]
14. Matzke, G. Verbindung von Wellen durch Verzahnung. *Konstruktion* **1951**, *3*, 211–216.
15. Croccolo, D.; De Agostinis, M.; Fini, S.; Olmi, G. Tribological properties of bolts depending on different screw coatings and lubrications: An experimental study. *Tribol. Int.* **2017**, *107*, 199–205. [CrossRef]
16. Croccolo, D.; De Agostinis, M.; Vincenzi, N. A contribution to the selection and calculation of screws in high duty bolted joints. *Int. J. Pres. Ves. Pip.* **2012**, *96*, 38–48. [CrossRef]
17. Croccolo, D.; De Agostinis, M.; Vincenzi, N. Influence of tightening procedures and lubrication conditions on titanium screw joints for lightweight applications. *Tribol. Int.* **2012**, *55*, 68–76. [CrossRef]
18. Croccolo, D.; De Agostinis, M.; Fini, S.; Olmi, G. An experimental study on the response of a threadlocker, involving different materials, screw dimensions and thread proportioning. *Int. J. Adhes.* **2018**, *83*, 116–122. [CrossRef]
19. Croccolo, D.; Vincenzi, N. Tightening tests and friction coefficients definition in the steering shaft of front motorbike suspension. *Strain* **2011**, *47*, 337–342. [CrossRef]
20. Niemann, G.; Winter, H.; Hohn, B.R. *Maschinenelemente*; Springer-Verlag: Berlin, Germany, 2005.
21. Croccolo, D.; De Agostinis, M.; Vincenzi, N. Normalization of the stress concentrations at the rounded edges of a shaft-hub interference fit: Extension to the case of a hollow shaft. *J. Strain Anal. Eng.* **2012**, *47*, 131–139. [CrossRef]
22. Croccolo, D.; De Agostinis, M.; Fini, S.; Morri, A.; Olmi, G. Analysis of the influence of fretting on the fatigue life of interference fitted joints. In Proceedings of the ASME International Mechanical Engineering Congress and Exposition, Montreal, QC, Canada, 14–20 November 2014; Volume 2B, p. V02BT02A008. [CrossRef]
23. Jiang, X.J.; Zhang, Y.Y.; Yuan, S.X. Analysis of the contact stresses in curvic couplings of gas turbine in a blade-off event. *Strength Mater.* **2012**, *44*, 539–550. [CrossRef]

24. Croccolo, D.; Cuppini, R.; Vincenzi, N. Friction coefficient definition in compression-fit couplings applying the DOE method. *Strain* **2008**, *44*, 170–179. [CrossRef]

25. RR71, Friction in Temporary Works, ISBN 0 7176 2613 X, HSE Books. Available online: http://www.hse.gov.uk/research/rrhtm/rr071.htm (accessed on 19 November 2018).